Open Peer Review on Qeios

Study Importance of Mutation in RAD50 Gene Based on in Silico Analysis of in Vivo Mutation

Nahid Khalili

Funding: No specific funding was received for this work.

Potential competing interests: No potential competing interests to declare.

Abstract

DNA repair processes occur in all species and the proteins involved are highly conserved. The MRN complex is one of the major sensors of braked DNA and RAD50 as part of the MRN complex supports allosteric connexions over long distances between the zinc hook and the coiled-coil domain. In this study Zebrafish were used as a model to study RAD50 mutation *in vivo*. Knock-out (KO) RAD50 embryos using CRISPR-Cas9 shows embryonic lethality. The final DNA Sanger sequence in each edited sample shows a nucleotide deletion (G) and a nucleotide insertion (A) in the target site, whereupon the aspartic acid residue (D) in the wild type was changed to an asparagine residue (N) in the edited sequences. By *in silico* analyses of the protein sequence, we found that the nucleotide change could cause a change in the amino acid and protein structure of RAD50 in Zebrafish.

Nahid Khalili

Department of Biological Sciences and Biotechnology, Faculty of Science and Technology, University Kebangsaan Malaysia, Bangi, Selangor, Malaysia

Keywords: Mutation, RAD50, *In silico*, CRISPR, Zebrafish.

1. Introduction

The cell has evolved different ways to repair the damaged DNA. Depending on the type of damage, specific pathways are activated for repair (Shibata et al. 2014). Homologous recombination (HR) is one of the several mechanisms active in double strand break (DSB) repair that are important for maintaining genome integrity. In addition to DSB repair, HR is also actively involved in cross-link repair, recovery of stalled replication forks, and telomere restoration. This pathway is mediated by proteins such as Ataxia telangiectasia mutated (ATM) and the Mre11/RAD50/Nbs1 (MRN) complex to repair DSBs. The MRN complex binds to the DNA DSB and then recruits ATM to the break site. ATM is activated by binding to the MRN complex and subsequently recruits other proteins involved in repair (M F Lavin 2007). The MRN complex is the

key protein complex involved in maintaining DNA loyalty and helps in DNA damage response (DDR). Mre11-RAD50 (MR) forms the core complex of MRN. The core complex is a heterotetramer and consists of two subunits each of Mre11 and RAD50. The association of the core complex with Nbs1 leads to the formation of the MRN complex (Martin F. Lavin et al. 2015; Situ et al. 2019). RAD50 is a protein with a size of 150 kDa, which contain zinc hook and coiled coil region. Mutations in the Human RAD50 zinc hook region involve significant defects associated with ATM activation, homologous recombination, susceptibility to irradiation, and activation of the ATR pathway. The zinc hook of RAD50 helps in holding the DSB ends of the chromosome, suggesting its role in preventing chromosome breakage (He et al. 2012). To regulate the downstream functions of RAD50, both the ATM and ATR kinases can phosphorylate it at serine 635. This is a highly specific single-site phosphorylation (Gatei et al. 2011). There are no other reported phosphorylation sites in RAD50 upon DNA damage. Mutants of this phospho site (S635G) in RAD50 show disruption of the S-phase checkpoint in RAD50-deficient cells and exhibit sensitivity to radiation. In response to DNA, S635 phosphorylation on RAD50 has been shown to be a prerequisite for ATM -dependent cell cycle regulation, DNA repair, and cell survival (Gatei et al. 2011). Voelkening et al. showed that fibroblasts that are RAD50-deficient exhibit "slow division". The phenotype can be rescued by complementation with both wild-type RAD50 and Ser635-mutated RAD50 (Völkening et al. 2020). Previous experiments have been performed with RAD50 mutations in vitro, which limits the scope for understanding the importance and function of the RAD50 protein in the morphological, physiological and structural development of animals. Mutations in the RAD50 gene have not been extensively studied in organisms. In this study, we aimed to investigate the effects of a RAD50 mutation on zebrafish development as an in vivo model.

2. Materials and methods

2.1. *Source of the gene sequences and pathogenic mutation variants*

The RAD50 genes of *Danio rerio* (Zebrafish) and *Homo sapiens* (Human) with GenBank accession id: XP_005167995.1 and AAB07119.1 respectively, were obtained from GenBank of National Centre of Biotechnology Information (NCBI) (http://www.ncbi.nlm.nih.gov).

The pathogenic RAD50 variants were compiled from a search with ClinVar (NCBI).

2.2. *Ethics statement and Zebrafish husbandry*

All *in vivo* experimental procedures were performed in accordance with the EU-directive 2010/ 63/EU on the protection of animals used for scientific purposes, and all procedures were carried out under project approval number: FST/2018/MOHD SHAZRUL/28-MAR.-2018-DEC.-2021, approved by the UKM Animal Ethical Committee.

All experiments were performed with a laboratory-bred zebrafish strain (AB). The zebrafish were housed in a room with a temperature of 28 °C and a 14-hour light and 10-hour dark cycle. The adult fish were fed once or twice daily with a mixture of ground flake food, brine shrimp and egg yolk. Adult fish were kept at a maximum density of one fish/200 ml. The adult

zebrafish were obtained from the Brain Research Institute Monash Sunway (BRIMS).

2.3. *Identification of target site of RAD50 in Zebrafish genome and preparation sgRNA*

In this study, RAD50 of *Danio rerio* Gene ID: 553029 was subjected for gene editing. The residue Ser635 site in protein was identified as a target site for the gene editing using http://chopchop.cbu.uib.no/. The closest and highly efficient target site was chosen. T7 promoter sequence (TAATACGACTCACTATA) added at the 5' to target sequence, and 20nt Overlapping crRNA-TracrRNA sequence (GTTTTAGAGCTAGAAATAGCat) the 3'. The final sequence (TAATACGACTCACTATACCAGTCAGACTTAAGCAAACGTTTTAGAGCTAGAAATAGCAAG) was prepared. The sgRNA DNA template synthesized by overlapping primers (Forward:5'-GTATACCGTCGACCTCTAGCTAGAGCTTGG-3' Reverse: 5'-AAAAAAGCACCGACTCGGTGCCACTTTTTCA-3'). The size of DNA template fragment were around 500 bp. In order to further verified the sequence of the template, the PCR products were subcloned into pMK-RQ vector and we chose E.coli K12 DH10B™ T1R colony to confirmed by Sanger's sequencing. The plasmid DNA was purified from transformed bacteria and concentration determined by UV spectroscopy. The final construct was verified by sequencing. The sequence congruence within the insertion sites was 100%. `1 In order to prepare *in vitro* synthesized sgRNA, the constructed plasmid was linearized *in vitro* transcribed by MEGAshortscript TM T7 Transcription Kit (#AM1354 Ambion) following the manufacturer's instructions. Using the MEGAclear package (# AM1908; Ambion), the prepared RNAs were purified and recovered in RNase-free HEPES-buffered saline (#H3537; Sigma-Aldrich Co., St. Louis, MO, USA).

2.4. *Microinjection of Zebrafish embryos*

All injections were performed in the wild-type strain of Zebrafish. To assure a high-efficiency delivery of the injected mRNA to the embryo as well as to reduce mosaicism, it was co-injected into 1-cell stage embryos. Embryos were injected with 600 (ng/µL) of Cas9 mRNA(Invitrogen A29378) and 200 (ng/µL) of sgRNA (RAD50) using a PicoPump. All the injection solutions had 5% of phenol red (Sigma) as a tracer and 160 mM of the isotonic solution Potassium Chloride (KCl). Was prepared 10 ul of injection solution, then injected ~ 1 ml of solution, which was measured with a millimetric ruler. The embryos grew in 1X E3 medium, which included Penicillin and Streptomycin (P0781, Sigma) at concentration 1:1000. Then, they were dechorionated with Pronase (Roche) for 1 hour in a concentration of 0.012mg/ml. Under a stereomicroscope over 72 hpf of development, the injected embryos were then phenotyped for morphological abnormalities.

2.5. *Genomic DNA extraction and Detection of CRISPR-Cas9 induced mutation*

To extract the genomic DNA, injected and uninjected embryos were incubated for 2 hours at 55ºC in 50 ul of lysis buffer (10mM Tris-HCl (pH 8.0), 1 mM EDTA, 50 mM KCl, 0.3% Tween-20, 0.3% NP-40 and 500 ug/ml proteinase K). Then, the solution was incubated at 100 °C for 10 min to inactivate proteinase K.

Extracted DNAs from single injected and uninjected embryos were used for PCR amplification. Designed a pair of primers (~30 bp in size) that amplifies a ~900 bp region spanning the gene deletion/insertion area using Integrated DNA

Technologies (IDT) primer design tool (https://sg.idtdna.com/pages/tools/primerquest). For the preparation of 50ul of PCR reaction, 25ul of 2Xpcrbio Taq Mix Red, 2ul of each primer in 10µM concentration (forward GTATCACGTCGACCTCTAGCTAGAGCTTGG and revers AAAAAAGCACCGACTCGGTGCCACTTTTTC), 500ng extracted genomic DNA from each sample and PCR grade dH2O were mixed. A standard thermocycler (Biometra T3 thermocycler, Jena, Germany) was used to conduct the PCR. The PCR conditions were as follows: initial denaturation (1 minute at 95 ° C), accompanied by 40 denaturation cycles (95 °C for 15 secs), annealing (59 °C for 15 secs) and extension (72 °C for 30 secs). These PCR products used to verification of DNA edition with Sanger sequencing.

2.6. *In silico analysis of mutated RAD50 protein*

To investigate the possible effect of edited DNA on protein structure, the*in silico* analysis on the model structure that obtained from I-Tasser were conducted. The predicted structures were viewed and edited using Chimera from University of California San Francisco (UCSF). A single-point mutation on residue was generated and the side chain rotamer was optimized. The steric clashes of residues that resulted from the mutation were further analyzed.

The MutantElect web application was used to*in silico* generation of electrostatic potential between the wild type protein and mutant. http://structuralbio.utalca.cl/mutantelec/

3. Results and discussion

3.1. *Clinical pathogen variant*

A list of pathogen variants was compiled from the Clinvar databases of the National Center for Biotechnology (NCBI). The predicted Human RAD50 secondary structure was used to determine the location of these Clinvar mutants. Figure 1 illustrates how the mutant number can be used to determine the position of the variants within the protein structure. Based on the significance of each of these structural modes (α-helix, strand and coiled), the significance of each mutant can be determined. The MRE11-RAD50-NBS1 complex plays a key role in the recognition and repair of defective DNA.Through interaction with other key members of the DNA damage response, the MRN complex is involved in various DNA damage repair pathways. Mutations in any member of the complex can lead to hypersensitivity to genotoxic agents, which in turn increases an individual's susceptibility to cancer. Recent research pointed to the role of the MRN complex in tumorigenesis and cancer treatment, and explored potential approaches for targeting this complex for cancer treatment. For the first time, the result of research on MRN showed that germline mutations of the RAD50 protein were associated with Human hereditary disease (Winqvist 2003). The limited increased risk of cancer could be associated with a single RAD50 mutation (Bian et al. 2019; Lin et al. 2016; Thompson et al. 2016; Waltes et al. 2009; Wang et al. 2008). In 2009, a patient with RAD50 deficiency was identified and described by Waltes et al. resulting in a first-time clinical phenotype that could be classified as NBS-like disease (NBSLD) (Waltes et al. 2009). Germline mutations in RAD50 (R1093X and Y1313X) cause NBS-like disorder (Syed & Tainer 2018). All observations demonstrate the relevance of genetic interaction research and functional analysis to further confirm findings from high-throughput screening mutation research.

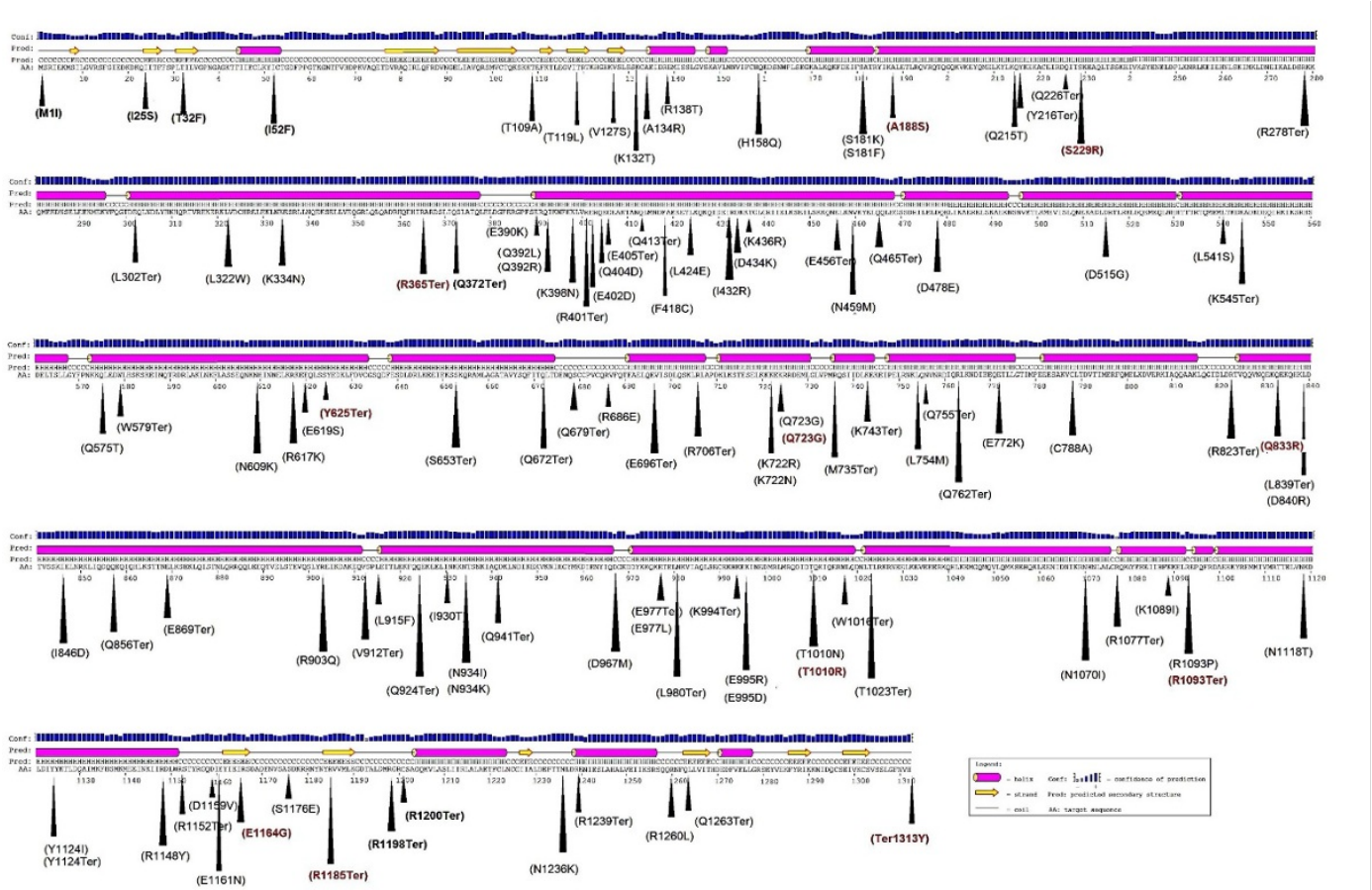

Figure 1. Summary of all 118 pathogenic clinical pathogen variant on RAD50. Nijmegen breakage syndrome-like disorder (NBSLD) shown in dark red colour.

3.2. *Phenotype of RAD50 knock-out Zebrafish embryos using CRISPR-Cas9*

The injected and non-injected embryos were counted and checked along with their morphology to assess the toxicity of RAD50 CRISPR. Any aberrant phenotypes, such as bent spine and tail, disrupted anterior-posterior axis, underdeveloped eyes, pericardial edoema, yolk edoema, microcephaly and missing head, have been prevalent (Figure 2.a). Previous studies have shown that CRISPR / Cas9 can induce biallelic mutations, and phenotypes can also be observed directly in injected embryos (F0) (Jao et al. 2013). To determine the effect of injection of CRISPR-Cas9 in the Zebrafish embryos lethality, the survival rate of the Zebrafishes was monitored after injection. In the injected RAD50.sgRNA group, the number of alieved embryos was reduced, and they could not survive after 72 hpf (figure 2.b). It was found that knockout of RAD50 consistently resulted in visible phenotypic abnormalities of the head. Out of the 60% of injected embryos, the head was normal in uninjected embryos but 10% of phenol red injected group displayed mild head abnormality. In RAD50.sgRNA injected group, two type of head abnormalities appeared; 50% mild abnormality and 10% severe head abnormality (head missing) displayed. This group could survive 50-58 hpf age (figure 2.c). For injected cases, severe microcephaly ($P < 0.0001$, $n = 10$ per injection) was frequently observed. It would allow direct phenotypic study in the injected embryos to produce robust biallelic mutations in the F0. Most of the developmental phenotypes, which are the

most dynamic forms of various disorders, affects the central nervous system (CNS). (Jao et al. 2013; Liu et al. 2017).

a

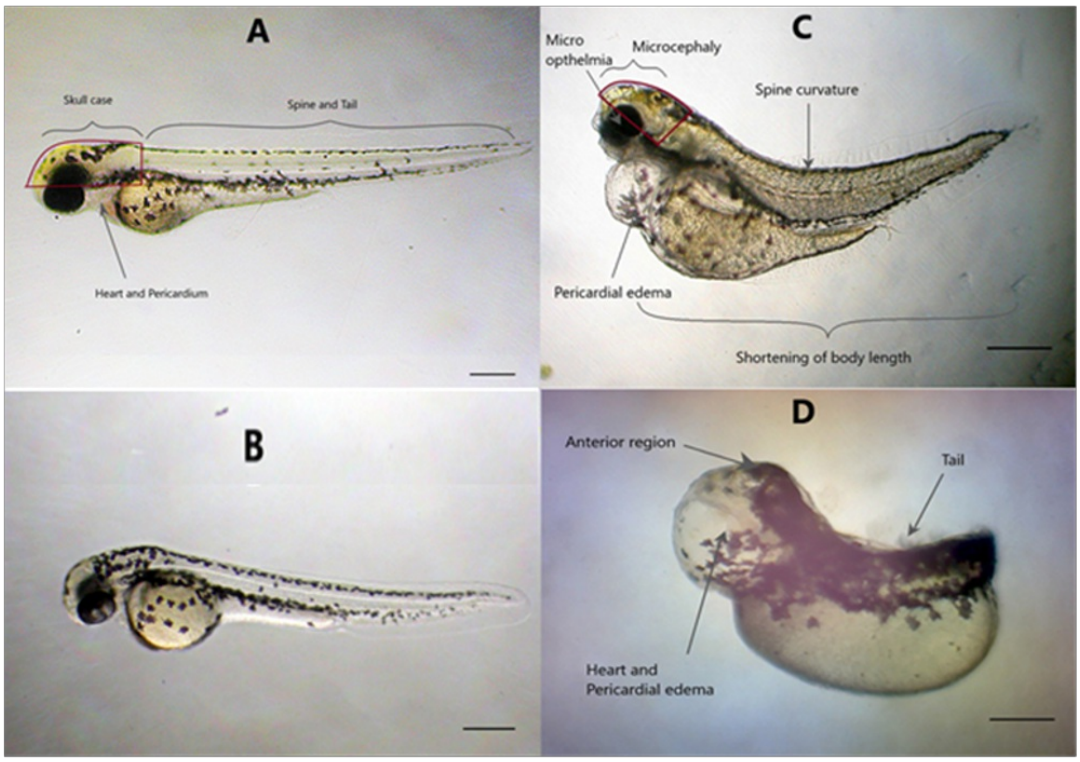
A
Skull case
Spine and Tail
Heart and Pericardium
C
Micro opthelmia
Microcephaly
Spine curvature
Pericardial edema
Shortening of body length
B
D
Anterior region
Tail
Heart and Pericardial edema

b

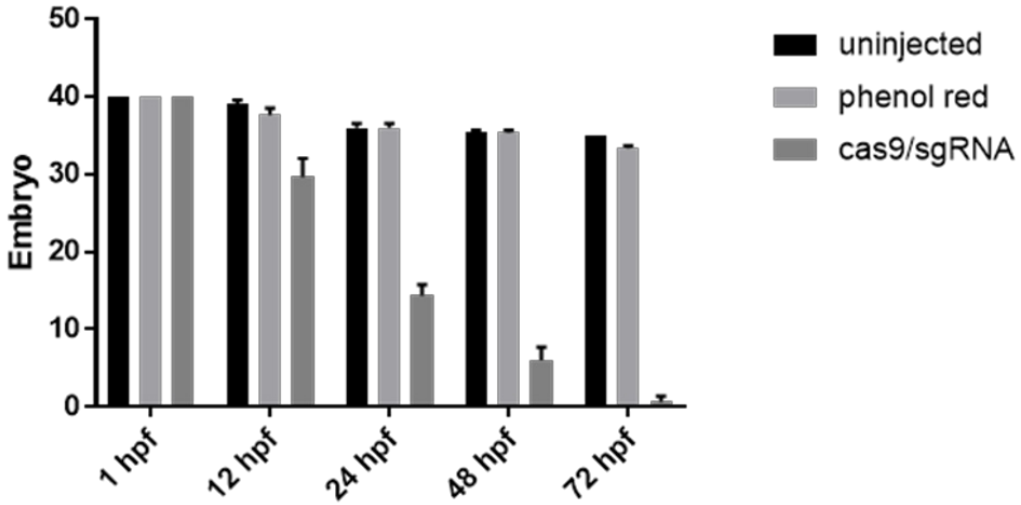
Embryo
50
40
30
20
10
0
1 hpf
12 hpf
24 hpf
48 hpf
72 hpf
uninjected
phenol red
cas9/sgRNA

c

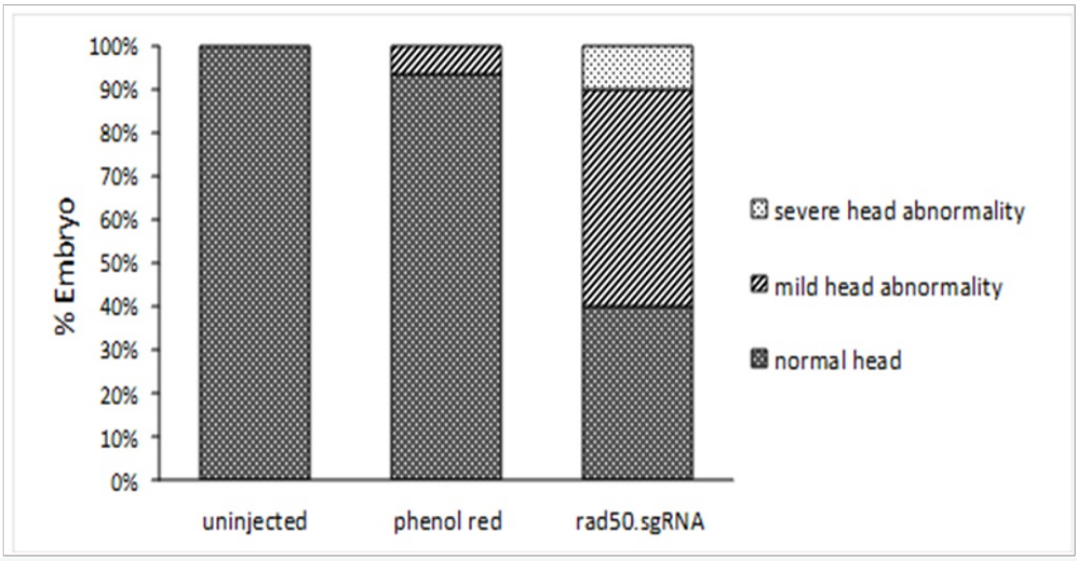
% Embryo
100%
90%
80%
70%
60%
50%
40%
30%
20%
10%
0%
uninjected
phenol red
rad50.sgRNA
severe head abnormality
mild head abnormality
normal head

Figure 2. RAD50 gene editing in Zebrafish by CRISPR-Cas9. **a**: Lateral views of A: non-injected B: injected (phenol red), C and D: injected (RAD50.sgRNA). AB Zebrafish embryo displays microcephaly(C) and head missing (D). The red line indicates the area of the skull. Magnification 4X. Scale bars: 100 µm. **b:** Survival rate of injected and uninjected embryos (CRISPR-Cas9), significant difference between groups (n=40, $p < 0.001$) **c:** Head abnormalities in affected Zebrafish embryos. The percentage of observed head phenotypic abnormalities for each group was scored at 48 hpf. n = 10 embryos per group. $p < 0.001$

3.3. *Detection of mutants – Genotyping*

The RAD50.sgRNA was injected into one-cell stage Zebrafish embryos. To test the efficiency of the injected CRISPR, DNA was extracted from injected RAD50.sgRNA embryos and uninjected Wild Type (WT) embryos. PCR was performed to amplify the region of interest. PCR product DNA was used for sequencing. Deleted and inserted indels, as we can see in figure 3, in comparison with wild type sequence and edited samples sequences is obvious. There were one nucleotide (G) was deleted and one nucleotide (A) was added. ICE online software was used to determine the efficiency in the edited samples. The editing efficiency was determined by comparing the edited trace to the control trace. In the ICE algorithm, potential editing outcomes are proposed and fitted to the observed data using linear regression. Each bar of the Indel plot showed the size of the insertion or deletion (±1 or more nucleotides), along with the percentage of genomes that contain it (Hsiau et al. n.d.). As shown in figure 4, out of the efficiency percentage calculated for eight edited samples, the highest percentage is 19. The Pearson correlation coefficient (R2) was also computed and reported. The higher R2 value was indicative the more confident in the ICE score (Jin et al. 2020).

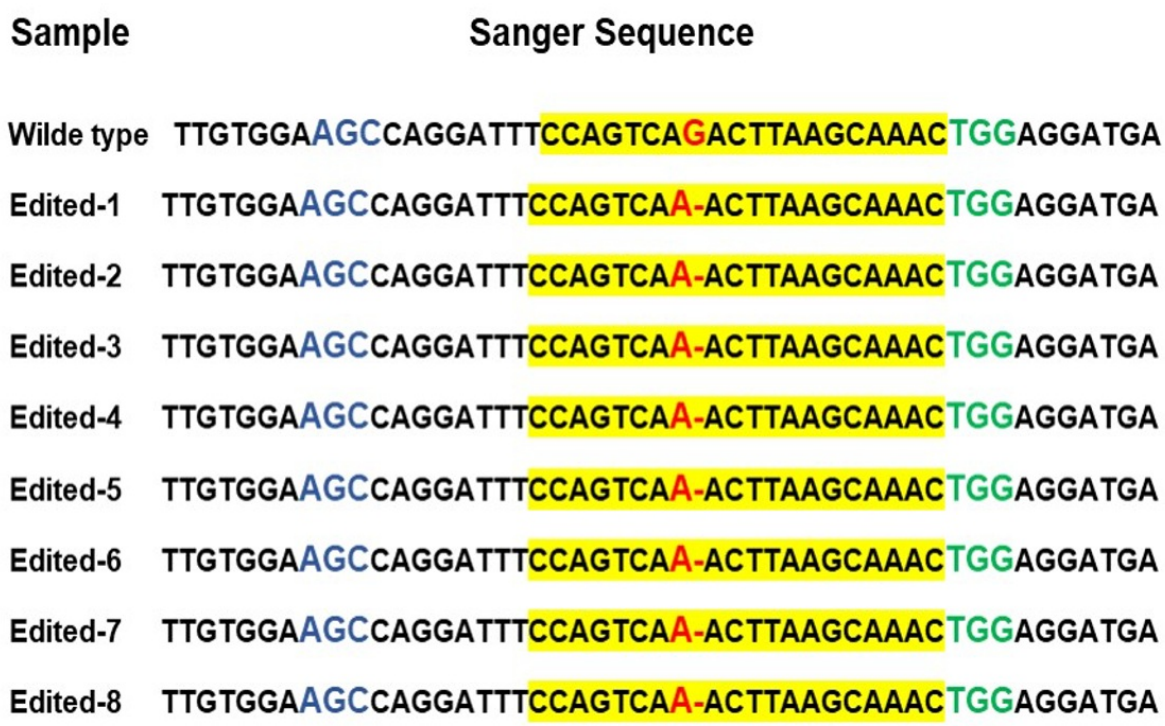

Figure 3. Representative Sanger sequencing findings show indels (red) induced by Cas9 / gRNA in the targeted locus of the PCR amplicons from 8 individual embryos at 24 hpf. (highlighted in yellow). 1 bp (G) was deleted, and 1 bp (A) added. TGG (green) is the PAM sequence. Ser635 phosphorylation site showed in blue.

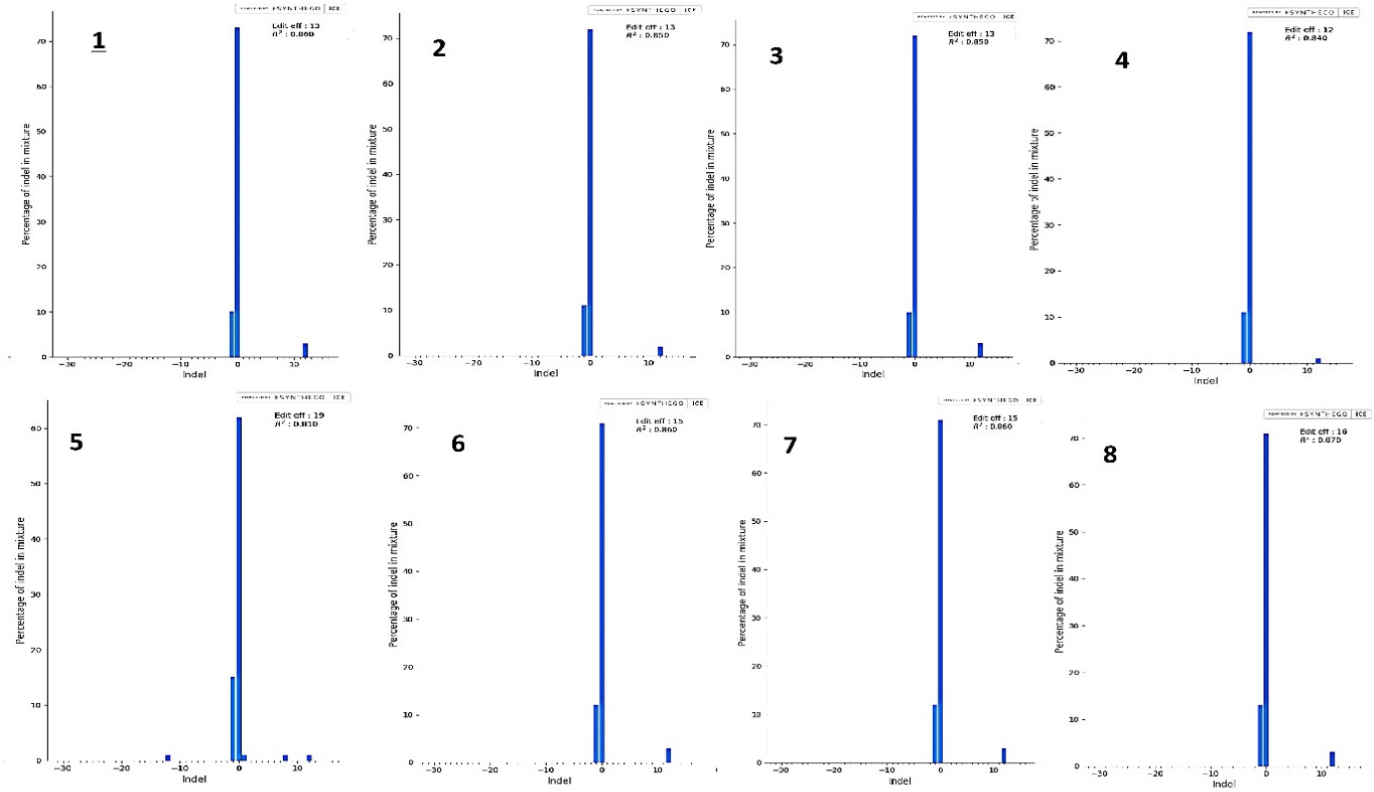

Figure 4. The Intel plot of edited samples. Each bar of the Indel plot shows the size of the insertion or deletion (+ or - 1 or more nucleotides), along with the percentage of genomes that contain it. Sample number 5 got highest bar size among total eight edited samples.

3.4. *In silico analyses edited RAD50*

The CRISPR/Cas9 system was used to generate mutations in RAD50. It is necessary to produce similar mutations in any cell of the animal for further phenotypic characterization. This can only be done after germline transmission of injected founder fish mutants. As mentioned in the previous sections, injected embryos with CRISPR (RAD50.sgRNA) did not grow after 72 hpf, so we could not achieve germline transmission of injected embryos. Analysis of Sanger sequence results, there was one nucleotide deletion (G) and insertion one nucleotide (A) in target site. These changes look like substitution in final DNA Sanger sequence in each edited sample. By *in silico* analyses of the protein sequence, we observed that the change in the nucleotide can cause a change in the amino acid. As we can see in figure 5, based on wild type sequence aspartic acid (D), the residue changed to asparagine (N) residue in the edited sequences.

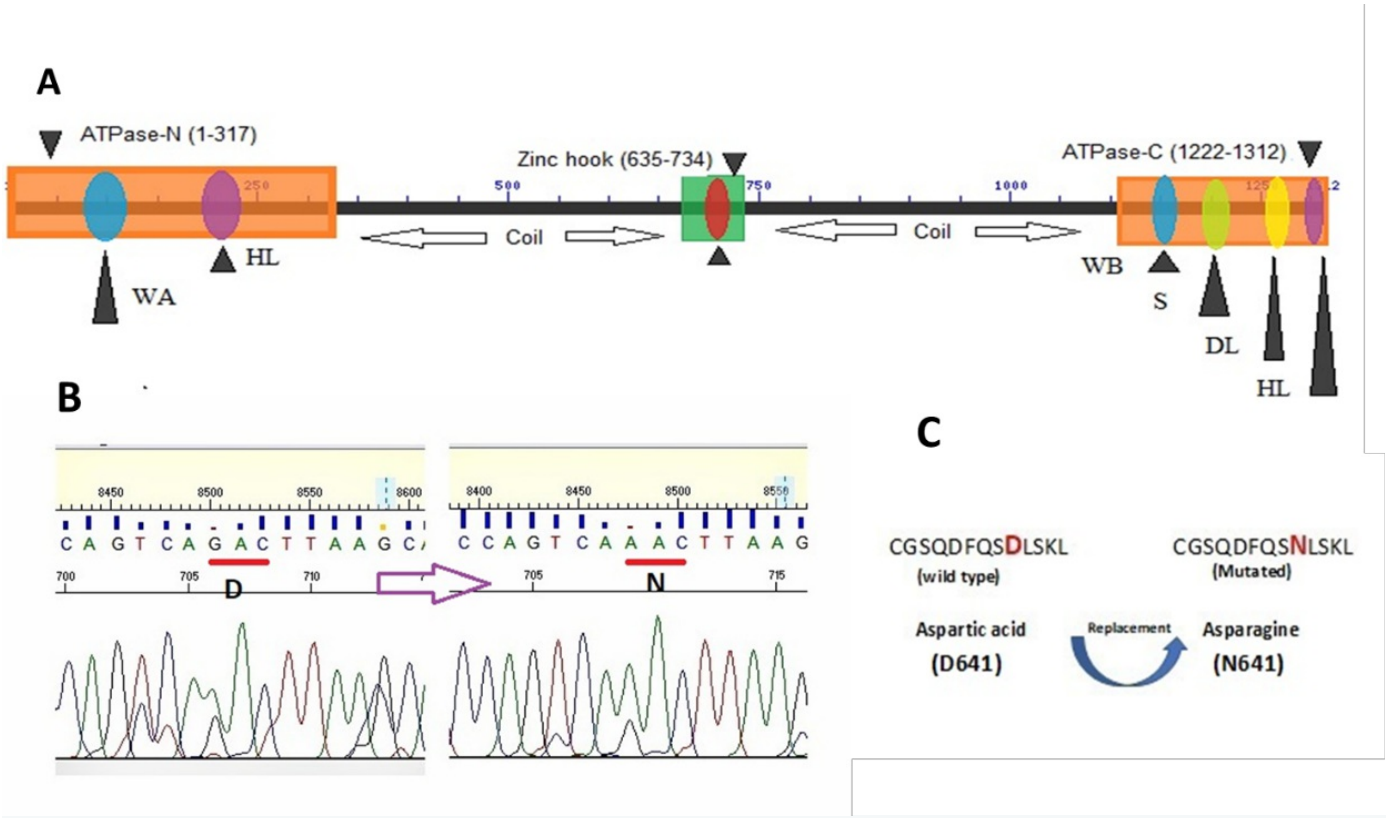

Figure 5. Representative single point mutation in edited samples. A) RAD50 sequence contain 1312 amino acid and domain analysis showed that RAD50_H.sapiens and RAD50_D.rerio contains three main domains which are ATP-binding cassette domain at each end of N and C terminal and RAD50 domain at the middle of the sequences. They have seven motifs which are; Walker A (WA) and Walker B (WB) motifs at either end of the protein, signature motif, Q loop (QL), D loop (DL) and H loop (HL). B and C Protein sequence of wild type and mutated embryo. Aspartic acid (D641) replaced with Asparagine (N641)

The UCSF chimera used to model the structure of Zebrafish RAD50, which has two type samples, those are, wildtype (non-injected) and mutated (injected). The residue of D641 was highlighted as green color (Figure 6A). In order to find and understand the clash, all atoms within 5 angstroms of the Asp641 were selected, and residue Aspartic acid641 was changed to residue Asparagine. Some significant changes in the local structure of the protein around the site of mutation were observed. Replacing Aspartic acid641 to Asparagine show no significant changes. After replacing the alternative, residues show all possible rotameric states. Clashes were checked to understand the reasons of changes after replacement of residue, and for replaced residue, the designated atoms against all other atoms were checked. The clashing atoms were highlighted on red and there were yellow pseudo board going only between Valin632.A and Asparagine 641.A (figure 6B). There were 5 clashes with Val632 residue, as we can see the yellow line indicates the hydrogen bonds, 1) VAL 632.A 1HG1-ASN 641.A OD1 1.568A°. 2) VAL 632.A CG1-ASN.A OD1 1.831A° 3) VAL 632.A 3HG1-ASN 641.A OD1 1.446A° 4) VAL 632.A 1HG1-ASN 641.A CG 1.903A° 5) VAL 632.A 1HG1-ASN 641.A CG 1.903A°.

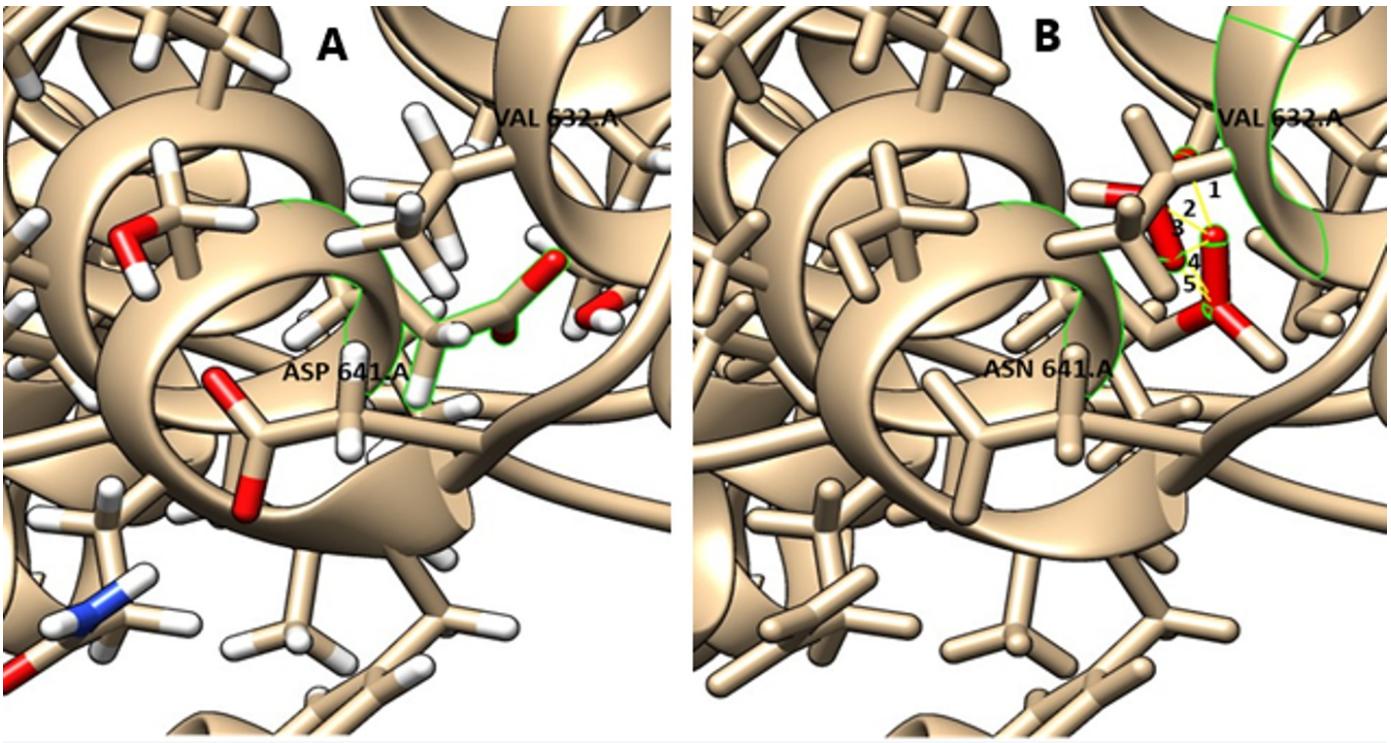

Figure 6. Homology modelling of mutation in ASP641 site of RAD50 protein of Zebrafish. A) wild type ASP641 and B) Mutant. Aspartic Acid replaced with Asparagine in 641 residue position and after replacement got clash with VAL632. The yellow line indicates the hydrogen bonds, 1) VAL 632.A 1HG1-ASN 641.A OD1 1.568A°. 2) VAL 632.A CG1-ASN.A OD1 1.831A° 3) VAL 632.A 3HG1-ASN 641.A OD1 1.446A° 4) VAL 632.A 1HG1-ASN 641.A CG 1.903A° 5) VAL 632.A 1HG1-ASN 641.A CG 1.903A°

To determine the atomic interactions of mutant amino acids with their side chains, the UCSF Chimera method was used (Pettersen et al. 2004). Clashes are unfavorable interactions in which atoms are very close to each other and collisions signify all sorts of direct interactions such as polar and non-polar, favorable and unfavorable. The mutated amino acid includes numerous rotamers, and the length of the side chain is closely correlated with the number of rotamers in the substituted amino acid. There are a certain number of inter-atomic collisions between each rotamer that can be defined as unique to the community. Asparagine642, which used the first rotamer with the highest likelihood number, has more than ten rotamers. Both of these rotamers may cause multiple phenotypes comparable to each other. (Banerjee et al. 2016). The position and type of a mutated residue affects the protein's stability due to mutation decrease, especially as the solvent accessibility of a residue decreases (Akhoundi et al. 2016). A missense mutation is a DNA error that results in the wrong amino acid being incorporated into a protein because the single DNA sequence is altered, resulting in a different codon of the amino acid known to the ribosome. Improvements in amino acids can be important in protein production. In most cases, however, they make little or no difference. The addition of amino acids is often caused by mutational errors, allowing the protein to do its job better.

MutantElec is an online programme for site-directed protein mutagenesis *in silico* generation and compares the electrostatic potential between the protein of the wild form and the mutant(s), depending on the three-dimensional protein structure. Figure 7 shows the effect of the mutation in RAD50 protein. It was evaluated by using a different approach to the traditional surface map. In this figure, Visualization of changes that arise at a near distance from the ASP-ASN641

displays the effect and therefore exposes the local and global influence of a particular transition. As we can see, with ASP->ASN641 and LEU642, there was a major gap in electrostatic potential. In determining the affinity of a ligand to a given protein target, electrostatic potential (EP) plays a key role and is responsible for many enzyme catalytic activities. (Valdebenito-Maturana et al. 2017). Mutation in residue can cause changes in surface steric clash, H-bonding and electrostatic potential. Change in surface electrostatic potential can prevent intersubunit interactions (Sarkar et al. 2014). However, these mutations evaluation require further investigations and validations.

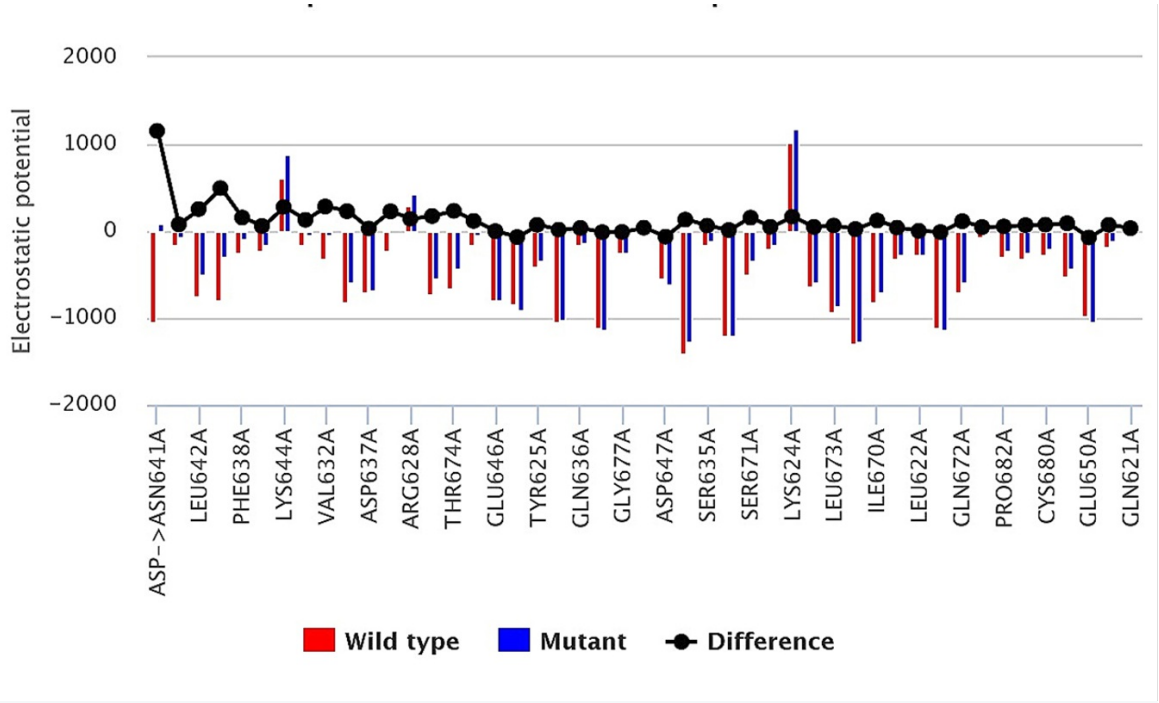

Figure 7. MutantElec analyses RAD50 protein in D641N. Combinatorial chart displaying the electrostatic potential of the input and mutant proteins, and the difference in potential between both. Aspartic acid (D641) replaced with Asparagine (N641)

4. Conclusion

This research included an output of zebrafish RAD50 results. The CRISPR-Cas9 technique is used to knockout RAD50 at the Ser635 phosphorylation site. Injected RAD50.sg.RNA embryos showed abnormalities such as microcephaly and did not survive after 72 hpf. Analysis of the sangar sequence of the mutant revealed that one bp (A) was added and one bp (G) was deleted. This change affected the protein sequence and Aspartic acid (D641) changed to Asparagine (N641). In silico analysis of the induced RAD50 protein showed a collapse of the 3D structure and a large difference in electrostatic potential (EP) between the wild-type and mutant strains. The results suggest that the RAD50 gene is important for the development of Zebrfish embryos in the early stages. In this study, we used ultrastructural studies to show that any change in the gene structure affects its function as a protein and can cause the diseases mentioned in the research.

Acknowledgments

We would like to thank to Dr. Satoshi Ogawa, Senior Lecturer at Monash University Malaysia, Brain Research Institute and Dr. Kazuhide Shaun Okuda at Cancer Research Initiatives Foundation Malaysia, whose contributions made this research possible. Financial support was obtained from the Ministry of Higher Education of Malaysia under the grant number 02-01-02-SF1279.

References

- Akhoundi, F., Parvaneh, N. & Modjtaba, E. B. 2016. In silico analysis of deleterious single nucleotide polymorphisms in human BUB1 mitotic checkpoint serine/threonine kinase B gene. *Meta Gene* 9: 142–150. doi:10.1016/j.mgene.2016.05.002
- Banerjee, S., Wu, Q., Ying, Y., Li, Y., Shirota, M., Neculai, D. & Li, C. 2016. In silico predicted structural and functional insights of all missense mutations on 2B domain of K1/K10 causing genodermatoses. *Oncotarget* 7(33): 52766–52780. doi:10.18632/oncotarget.10599
- Bian, L., Meng, Y., Zhang, M. & Li, D. 2019. MRE11-RAD50-NBS1 complex alterations and DNA damage response: Implications for cancer treatment. *Molecular Cancer*. BioMed Central Ltd. doi:10.1186/s12943-019-1100-5
- Gatei, M., Jakob, B., Chen, P., Kijas, A. W., Becherel, O. J., Gueven, N., Birrell, G., et al. 2011. ATM protein-dependent phosphorylation of Rad50 protein Regulates DNA repair and cell cycle control. *Journal of Biological Chemistry*. doi:10.1074/jbc.M111.258152
- He, J., Shi, L. Z., Truong, L. N., Lu, C. S., Razavian, N., Li, Y., Negrete, A., et al. 2012. Rad50 zinc hook is important for the Mre11 complex to bind chromosomal DNA double-stranded breaks and initiate various DNA damage responses. *Journal of Biological Chemistry* 287(38): 31747–31756. doi:10.1074/jbc.M112.384750
- Hsiau, T., Maures, T., Waite, K., Yang, J., Kelso, R., Holden, K. & Stoner, R. (n.d.). Inference of CRISPR Edits from Sanger Trace Data. doi:10.1101/251082
- Jao, L.-E., Wente, S. R. & Chen, W. 2013. Efficient multiplex biallelic zebrafish genome editing using a CRISPR nuclease system. *Proceedings of the National Academy of Sciences* 110(34). doi:10.1073/pnas.1308335110
- Jin, J. I., Xu, Y., Huo, L., Ma, L., Scott, A. W., Pool Pizzi, M., Li, Y., et al. 2020. An improved strategy for CRISPR/Cas9 gene knockout and subsequent wildtype and mutant gene rescue. doi:10.1371/journal.pone.0228910
- Lavin, M F. 2007. ATM and the Mre11 complex combine to recognize and signal DNA double-strand breaks *Oncogene* 26: 7749–7758. doi:10.1038/sj.onc.1210880
- Lavin, Martin F., Kozlov, S., Gatei, M. & Kijas, A. W. 2015. ATM-dependent phosphorylation of all three members of the MRN complex: From sensor to adaptor. *Biomolecules* 5(4): 2877–2902. doi:10.3390/biom5042877
- Lin, P. H., Kuo, W. H., Huang, A. C., Lu, Y. S., Lin, C. H., Kuo, S. H., Wang, M. Y., et al. 2016. Multiple gene sequencing for risk assessment in patients with early-onset or familial breast cancer. *Oncotarget* 7(7): 8310–8320. doi:10.18632/oncotarget.7027
- Liu, J., Zhou, Y., Qi, X., Chen, J., Chen, W., Qiu, G., Wu, Z., et al. 2017. CRISPR/Cas9 in zebrafish: an efficient combination for human genetic diseases modeling. *Human Genetics* 136(1): 1–12. doi:10.1007/s00439-016-1739-6
- Pettersen, E. F., Goddard, T. D., Huang, C. C., Couch, G. S., Greenblatt, D. M., Meng, E. C. & Ferrin, T. E. 2004.

UCSF Chimera - A visualization system for exploratory research and analysis. *Journal of Computational Chemistry* 25(13): 1605–1612. doi:10.1002/jcc.20084

- Sarkar, D., Ray, K. & Sengupta, M. 2014. Structure-function correlation analysis of connexin50 missense mutations causing congenital cataract: Electrostatic potential alteration could determine intracellular trafficking fate of mutants. *BioMed Research International* 2014. doi:10.1155/2014/673895
- Shibata, A., Moiani, D., Arvai, A. S., Perry, J., Harding, S. M., Genois, M.-M., Maity, R., et al. 2014. DNA Double-Strand Break Repair Pathway Choice Is Directed by Distinct MRE11 Nuclease Activities. *Molecular Cell* 53(1): 7–18. doi:10.1016/J.MOLCEL.2013.11.003
- Situ, Y., Chung, L., Lee, C. & Ho, V. 2019. MRN (MRE11-RAD50-NBS1) Complex in Human Cancer and Prognostic Implications in Colorectal Cancer. *International Journal of Molecular Sciences* 20(4): 816. doi:10.3390/ijms20040816
- Syed, A. & Tainer, J. A. 2018. The MRE11–RAD50–NBS1 Complex Conducts the Orchestration of Damage Signaling and Outcomes to Stress in DNA Replication and Repair. *Annual Review of Biochemistry* 87(1): 263–294. doi:10.1146/annurev-biochem-062917-012415
- Thompson, E. R., Rowley, S. M., Li, N., McInerny, S., Devereux, L., Wong-Brown, M. W., Trainer, A. H., et al. 2016. Panel testing for familial breast cancer: Calibrating the tension between research and clinical care. *Journal of Clinical Oncology* 34(13): 1455–1459. doi:10.1200/JCO.2015.63.7454
- Valdebenito-Maturana, B., Reyes-Suarez, J. A., Henriquez, J., Holmes, D. S., Quatrini, R., Pohl, E. & Arenas-Salinas, M. 2017. Mutantelec: An In Silico mutation simulation platform for comparative electrostatic potential profiling of proteins. *Journal of computational chemistry* 38(7): 467–474. doi:10.1002/jcc.24712
- Völkening, L., Vatselia, A., Asgedom, G., Bastians, H., Lavin, M., Schindler, D., Schambach, A., et al. 2020. RAD50 regulates mitotic progression independent of DNA repair functions. *The FASEB Journal* 34(2): 2812–2820. doi:10.1096/fj.201902318R
- Waltes, R., Kalb, R., Gatei, M., Kijas, A. W., Stumm, M., Sobeck, A., Wieland, B., et al. 2009. Human RAD50 deficiency in a Nijmegen breakage syndrome-like disorder. *American journal of human genetics* 84(5): 605–16. doi:10.1016/j.ajhg.2009.04.010
- Wang, X., Szabo, C., Qian, C., Amadio, P. G., Thibodeau, S. N., Cerhan, J. R., Petersen, G. M., et al. 2008. Mutational analysis of thirty-two double-strand DNA break repair genes in breast and pancreatic cancers. *Cancer Research* 68(4): 971–975. doi:10.1158/0008-5472.CAN-07-6272
- Winqvist, R. 2003. susceptibility Key points. *Molecular and Cellular Biology* 1–7.